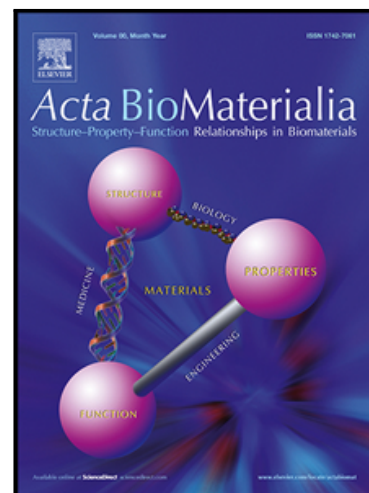


Interpenetrating polymer networks of collagen, hyaluronic acid, and chondroitin sulfate as scaffolds for brain tissue engineering

Fangxin Li , Martin Ducker , Bin Sun , Francis G Szele ,
Jan T Czernuszka

PII: S1742-7061(20)30321-4
DOI: <https://doi.org/10.1016/j.actbio.2020.05.042>
Reference: ACTBIO 6762



To appear in: *Acta Biomaterialia*

Received date: 14 February 2020
Revised date: 27 May 2020
Accepted date: 28 May 2020

Please cite this article as: Fangxin Li , Martin Ducker , Bin Sun , Francis G Szele , Jan T Czernuszka , Interpenetrating polymer networks of collagen, hyaluronic acid, and chondroitin sulfate as scaffolds for brain tissue engineering, *Acta Biomaterialia* (2020), doi: <https://doi.org/10.1016/j.actbio.2020.05.042>

This is a PDF file of an article that has undergone enhancements after acceptance, such as the addition of a cover page and metadata, and formatting for readability, but it is not yet the definitive version of record. This version will undergo additional copyediting, typesetting and review before it is published in its final form, but we are providing this version to give early visibility of the article. Please note that, during the production process, errors may be discovered which could affect the content, and all legal disclaimers that apply to the journal pertain.

Interpenetrating polymer networks of collagen, hyaluronic acid, and chondroitin sulfate as scaffolds for brain tissue engineering

Fangxin Li¹, Martin Ducker², Bin Sun², Francis G. Szele^{2*} and Jan T. Czernuszka^{1*}

¹ Department of Materials, University of Oxford, Oxford UK, OX1 3PH

² Department of Physiology, Anatomy and Genetics, University of Oxford, Oxford, UK, OX1 3QX

FGS: Corresponding Author – pre-publication

*Co-communicating Authors – post-publication

Francis G. Szele, PhD
Department of Physiology, Anatomy and Genetics
University of Oxford
South Parks Road
Oxford, UK
OX1 3QX
Francis.Szele@dpag.ox.ac.uk

Jan T. Czernuszka, PhD
Department of Materials
University of Oxford
Parks Road
Oxford, UK
OX1 3PH
Jan.czernuszka@materials.ox.ac.uk

Abstract

Stem cells can provide neuro-protection and potentially neuro-replacement to patients suffering from traumatic brain injuries (TBI), with a **practical** option being delivery via engineered scaffolds. Collagen (Coll) and glycosaminoglycan (**GAG**) have been used as scaffolds for brain tissue engineering yet they often do not support cell differentiation and survival. In this study, we developed interpenetrating polymer network scaffolds comprising Coll, and incorporating two commonly found GAGs in the brain, chondroitin sulfate (CS) and/or hyaluronic acid (HA). We seeded these scaffolds with mouse neural stem cells from the subventricular zone (SVZ) niche. Compared to Coll-alone, all other substrates decreased the percent of nestin+ stem cells. **Coll-CS-HA was more efficient at suppressing nestin expression than the other scaffolds; all SVZ cells lost nestin expression within 7 days of culture. In contrast to nestin, the percentage of microtubule associated protein 2 (MAP2+) neurons was greater in scaffolds containing, CS, HA**

or CS-HA, compared to Coll alone. Finally, Coll-CS increased the percentage of glial fibrillary acidic protein (GFAP+) astrocytes compared to Coll scaffolds. Overall, this work shows that Coll-HA and Coll-CS-HA scaffolds selectively enhance neurogenesis and may be advantageous in tissue engineering therapy for TBI.

Keywords: scaffold, subventricular zone, collagen, chondroitin sulfate, hyaluronic acid

Statement of Significance

Brain injury is devastating yet with few options for repair. Stem cells that reside in the subventricular zone (SVZ) only repair damage inefficiently due to poor control of their cellular progeny and unsuitable extracellular matrix substrates. To solve these problems, we have systematically generated collagen (Coll) scaffolds with interpenetrating polymer networks (IPN) of hyaluronic acid (HA) or chondroitin sulfate proteoglycans (CS) or both. The scaffolds had defined pore sizes, similar mechanical properties and all three stimulated neurogenesis, whereas only CS stimulated astrocyte genesis. Overall, this work suggests that Coll-HA and Coll-CS-HA scaffolds selectively enhance neurogenesis and may be advantageous in tissue engineering therapy for brain repair.

1. Introduction

The central nervous system (CNS) is a vulnerable system and is subject to traumatic brain injury (TBI). Approximately 2% of the US population are affected by disability resulting from TBI, and there are over 300,000 admissions annually in the UK for acquired brain injuries [1, 2]. Patients suffering from TBI will often experience loss of functions such as memory, movements and cognition. In severe cases, TBI is fatal [3, 4]. Recovery from these injuries is often difficult due to the inability of mature neurons to regenerate. Many studies have focused on transplanting neural stem cells (NSC), fetal tissue explants, engineered scaffolds and recently, cerebral organoids [5-12]. However, these studies often encounter problems including low cell viability, low neuronal differentiation, and high batch-to-batch variability [5-12]. The discovery of adult neurogenesis in the subventricular zone (SVZ), which lines the lateral ventricles has provided great hope for a potential therapy to regenerate lost tissue. After brain injury, SVZ cells proliferate at greater rates and doublecortin+ (Dcx+) newborn neurons migrate actively towards TBI, signifying an intrinsic attempt at repair [13-15]. However, the repair is insufficient and many groups are seeking interventions to augment this natural brain reparative process.

The purpose of a scaffold in tissue engineering is to mimic the extracellular matrix (ECM) of the tissue, providing mechanical support as well as chemical instructions. The major components within the human brain ECM are hyaluronic acid (HA), chondroitin sulfate proteoglycans (CSPG) and heparin sulfate proteoglycans. HA and CSPG are most commonly found in the neural interstitial matrix and in perineuronal nets [16]. HA is highly expressed in the SVZ and in the rostral migratory stream (RMS), the newborn neuron pathway to the olfactory bulbs, their normal destination [17]. It is important to note that CSPG is also expressed in the SVZ and RMS [18] and thus scaffolds made of it and HA could be ideal for culture and transplantation. The RMS exists in human infants [19] but has been controversial in adults [20, 21]. HA also accumulates around the lesion area of a photothrombotic stroke into which neurons migrate [17].

Functionally, HA supports cell differentiation, activates cell receptors for growth, [22] and participates in inhibiting scar formation [23]. On the other hand, CSPG promotes glial scar formation after brain injury. CSPGs are significantly upregulated by astrocytes and form a large portion of the glial scar, which inhibits neurite outgrowth and thus regeneration [24]. Previous studies digested CSPG using chondroitinase ABC (chABC) and showed that removal of the glial scar enhanced axonal spouting [25]. In contrast, CSPGs implanted into a TBI increased Dcx+ cell numbers, proliferation, brain-derived neurotrophic factor (BDNF) and glia-derived neurotrophic factor (GDNF) expression [26]. BDNF is a regulator of adult CNS synapses whereas GDNF is a neurotrophic factor that enhances neurite outgrowth. Hence, it is difficult to generate a conclusive statement on the effectiveness of CS as a potential scaffold for CNS tissue engineering. Furthermore, the combined effects of HA and CS are not well understood. Published studies using Coll-based scaffolds for TBI treatment thus far lack direct comparison of the effects of HA and CS on brain tissue engineering [26-28].

Here, we fabricated three interpenetrating network (IPN) scaffolds: collagen with chondroitin sulfate proteoglycan (Coll-CS), collagen with hyaluronic acid (Coll-HA) and collagen with chondroitin sulfate proteoglycan and hyaluronic acid (Coll-CS-HA) to study their physical and biological properties for brain tissue engineering and to compare them with collagen (Coll) scaffolds. Synthesis of the IPN was successful in incorporating GAGs onto the Coll structure while maintaining similar mechanical properties. Biologically, Coll-GAG scaffolds increased neuronal differentiation from SVZ NSCs compared to Coll. We also demonstrated that the IPNs reduced nestin expression with Coll-CS-HA resulting in complete loss a Day 7 and on. Finally, Coll-CS promoted astrocytic differentiation compared to Coll.

2. Materials and Methods

Fabrication of Coll and IPN scaffolds

Coll scaffolds were prepared from type I Coll from bovine Achilles tendon (Sigma Aldrich, C9879) via a freeze-drying method. 0.75g or 1.0g of Coll slurries were mixed with 100 mL water in an ice bath to form 0.75wt% or 1.0wt% Coll suspensions. The pH was adjusted to 3.2-3.5 by dropwise addition of ethanoic acid. The mixture was blended by a household blender (Breville, IHB086), followed by 5 mins' centrifugation at 2,500 rpm (relative centrifugal force = 1,015g) to remove trapped air bubbles (Thermo, IEC CL10). The mixture was then refrigerated at 4°C overnight for the solution to diffuse and become homogeneous again, followed by casting in cylindrical PTFE moulds (8 mm diameter, 15 mm height) and frozen in a -80°C freezer (Sanyo, Ultra Low Freezer) for at least 4 hrs. Subsequently, the mixture was freeze-dried in a Christ Alpha I-5 freeze-dryer for 24 hrs.

Coll-HA scaffold was formed via an EDC/NHS crosslinking approach. Freeze dried 0.75wt% Coll scaffolds were stirred in absolute ethanol for 30 mins. An HA crosslinking solution containing 0.25wt% sodium hyaluronate ($M_w = 1.5\text{-}2.2$ MDa, ACROS Organics, 9067-32-7), 60 mM N-ethyl-N'-(3-dimethylaminopropyl)carbodiimide hydrochloride (EDC) (Sigma Aldrich, 25952-53-8), 30mM N-hydroxysuccinimide (NHS) (Sigma Aldrich, 6066-82-9), 30 molar excess (of HA) adipic acid dehydrate (ADH) (Sigma Aldrich, 1071-93-8), and 50 mM 2-morpholinoethane sulfonic acid (MES) hydrate (Sigma Aldrich, 1266615-59-1) was allowed to react for 4 hrs on a stirrer at room temperature, and subsequently stored in a 4°C refrigerator for

a minimum of 12 hrs before adding Coll. ADH functionalised HA by addition of NH_2 bonds onto HA molecules, which were then crosslinked to their carboxylic groups to form a secondary network. To add the HA network onto Coll, 0.75wt% scaffolds were immersed in the crosslinking solution for 4 hrs, washed once in 0.1M Na_2HPO_4 solution for 1 hr, twice in distilled water for 1 hr, frozen at -80°C and then freeze-dried for 24 hrs.

Coll-CS scaffolds were synthesised via a similar approach. 0.75wt% Coll scaffolds were mixed with absolute ethanol for 30 min to dehydrate, then immersed in a CS (chondroitin-6 sulfate sodium salt from shark cartilage, Sigma-Aldrich, C4384) secondary network solution consisting of 0.25wt% CS, 60 mM EDC, 30 mM NHS, 30 molar excess (of CS) ADH, and 50 mM MES hydrate for 4 hrs on a stirrer at room temperature. The crosslinking solution has been previously reacting for 4 hrs to form the secondary network and stored in a 4°C fridge for a minimum of 12 hrs. The scaffolds were then washed and freeze-dried via the same way as Coll-HA.

Coll-CS-HA scaffolds were synthesised by adding ethanol-dehydrated 0.75wt% Coll scaffolds to a HA-CS crosslinking solution containing 0.25wt% HA, 0.25wt% CS, 60 mM EDC, 30 mM NHS, 50 mM MES, 30 molar excess (of CS and HA) ADH, and ADH for 4 hrs. This solution, again, has been reacting and kept in the same condition as above. The scaffolds were then washed and freeze-dried. All other Methods described in the Supplementary Materials.

Statistical analysis

Results are presented as mean \pm standard deviation. Student's unpaired t-test carried out in GraphPad were used for comparison between two groups and one-way ANOVA for comparisons between three or more groups were used to determine the statistical significance of differences between sets of data. $P < 0.05$ was used to determine significance. $N=3$ experiments were used for all studies were taken unless otherwise stated.

Results

3.1 Morphology and pore size of Coll and IPNs

SEM images of the cross-sections of 1.0wt% Coll and IPNs are shown in Fig. 1A and B. All IPN scaffolds were synthesised based on 0.75wt% Coll scaffolds. Images in panels A and B were taken at different magnifications to reveal their overall and internal pore structure.

Our results clearly showed that all IPNs exhibited highly porous foam-like structures similar to that of Coll. The freeze-drying process was effective in producing a highly porous structure. The pores were interconnected, allowing infiltration of cell culture media nutrients, growth and expansion of NSCs, and intermingling between cell colonies. When CS and HA were added, their pore structure became more distorted, as evidenced by extensive side-branches within the primary pores.

Fig. 1B shows a more distorted pore structure and an extensive growth of struts that led to a formation of secondary pores (arrowheads) on Coll-CS-HA. The original Coll structure was still observable by the thicker walls between the primary pores. Hence, it is implied that the growth of secondary pores has led to a reduction in the average pore size of Coll-CS-HA.

For 1.0% Coll, the pore size was defined by the size of ice crystals formed in the -80°C freezer. IPNs were based on 0.75% Coll, and the addition of CS and/or HA onto 0.75% Coll would create

secondary pores within the Coll primary network. It was indeed shown in Fig. 1C that the addition of CS and HA together had significantly reduced the pore size of Coll-CS-HA. Fig. 1C-F show the comparative pore sizes of the four scaffolds.

All scaffolds were in the optimal pore diameter range suitable for NSC culture, allowing both easy infiltration of cells as well as adequate cell-scaffold interaction in a 3D environment [33][29]. The differences between Coll, Coll-CS and Coll-HA were not determined to be significant, although the average pore size of Coll-CS was roughly $139 \pm 9 \mu\text{m}$ compared to Coll of $104 \pm 14 \mu\text{m}$. Coll-HA had a very similar pore diameter to Coll of $96 \pm 38 \mu\text{m}$, although its pores were more distorted, as evidenced by a larger standard deviation. Addition of CS and HA simultaneously however, had led to an extensive growth of struts and secondary pores within the Coll structure, which in turn reduced the average pore diameter to approximately $41 \pm 5 \mu\text{m}$.

3.2 Fourier-transformed infrared spectroscopy

Spectra of the IPNs were similar to that of Coll as shown in Fig. 2A. Superimposed FTIR spectra revealed that the IPNs caused amide I and II of Coll to shift slightly to lower frequencies (Fig. 2C), and a decreased absorption in Fig. 2C and Fig. 2D. In this case, such peak shifts are most likely due to changes in relative intensities of adjacent peaks, resulting in the overlapping peaks appearing to be shifted.

Apart from the $1078\text{--}1080 \text{ cm}^{-1}$ peak on Coll and Coll-HA, another peak was found on Coll-CS and Coll-CS-HA near 1061 cm^{-1} shown in Fig. 2B. This was due to the highly sulfated GAGs, which was CS in this case [30]. The increase in peak intensities of all IPNs, especially Coll-HA and Coll-CS-HA at around 1080 cm^{-1} region, also reflected the carboxylic groups of the uronic acid moiety of GAGs [31]. Coll-CS-HA had the highest intensity here, which was most likely due to the addition of HA and CS together. Between 1000 cm^{-1} and 1140 cm^{-1} , Coll-CS and Coll-CS-HA both had higher intensities compared to Coll and Coll-HA. Coll-CS-HA had the highest intensity, indicating a higher concentration of the polysaccharides [32].

Shown in Fig. 2E, the broad bands around 3200 cm^{-1} to 3400 cm^{-1} , centred at 3315 cm^{-1} , were due to the O-H stretching mode of polysaccharides and N-H stretching vibration of the N-acetyl side chain. During crosslinking, hydrogen bonds were formed by joining C=O on HA and CS with N-H on ADH-modified HA or joining C=O on Coll with N-H on Coll. This formation broadened the bands around this region, and was also reflected in Fig. 2e. Coll-CS-HA did not show an increase but a somewhat narrower band here [31]. This was due to the prior crosslinking which took place between CS and ADH-modified HA before the addition of Coll.

Fig. 2F illustrates the second derivatives curves of Coll and IPNs between 800 cm^{-1} and 1800 cm^{-1} . Typical Coll peaks were again obvious, as shown in 1628 cm^{-1} , which corresponded to amide I, in 1549 cm^{-1} , which corresponded to amide II, and in 1339 cm^{-1} , which corresponded to CH_2 side chain vibration [33]. These peaks were found in all IPNs, further validating our previous finding that the original Coll structure remained unchanged.

In addition, S-O-C bonds were found on Coll-CS and Coll-CS-HA at around $858\text{--}862 \text{ cm}^{-1}$. Peaks at this area shifted away from Coll and Coll-HA. S-O-C is a characteristic bond of CS, indicating the presence of CS within Coll-CS and Coll-CS-HA. Unsurprisingly, Coll-HA overlaps with Coll around this region.

Overall, Coll-CS-HA showed higher peak intensities in second derivatives. Coll-CS and Coll-CS-HA also showed a slight shift to lower wavenumber at the amide II peak, which was consistent with the FTIR findings. Peaks of Coll-HA however, did not show any significant differences compared to Coll.

Band assignments for secondary derivatives are shown in Table S3. As mentioned previously, band shifts of 4 cm^{-1} were deemed significant. Compared to Coll, a number of significant shifts from Coll-CS were seen, namely at amide I (-6 cm^{-1}), CH_3 asymmetric bending ($+4\text{ cm}^{-1}$ and -6 cm^{-1}), amide III (-4 cm^{-1}), and C-O-S asymmetric stretching ($+13\text{ cm}^{-1}$). Similarly, Coll-CS-HA also caused several peak shifts at amide II (-12 cm^{-1}) and C-O-S asymmetric stretching ($+9\text{ cm}^{-1}$). Coll-HA on the other hand, did not shift extensively at these peaks.

The ratio of pyrolidonic ring and amide III provided information about the denaturation of Coll triple helix, as pyrolidonic rings stabilises the secondary structure of Coll. Table S4 shows similar ratios of amide III (1244 cm^{-1}) to pyrolidonic ring (1452 cm^{-1}) of the IPNs to Coll as GAGs were added. Ratios for all scaffolds were around 1, which is consistent with previous findings [34]. Denatured Coll triple helix has an amide III/pyrolidonic ring ratio of approximately 0.6 [35]. These results clearly showed that the IPNs synthesis method well preserved the original Coll triple helix structure, avoiding the degradation of collagen.

Fig. 3 illustrates the compressive modulus of porous scaffolds. The elastic modulus of Coll-CS-HA in a foam phase was 27.9 kPa , which was statistically significantly higher than those of Coll, Coll-CS and Coll-HA, whose modulus were 14.6 kPa , 16.3 kPa and 16.8 kPa respectively. As expected, when densities of scaffolds were considered and taken into the Gibson- Ashby equations, there was no significant differences between the interlaced scaffolds and Coll, as illustrated by Fig. 3A. While the exponent equalled to $3/2$, the normalised compressive moduli of the solid phases of Coll-CS, Coll-HA and Coll-CS-HA were 0.93 ± 0.02 , 0.84 ± 0.21 and 0.93 ± 0.14 . Coll-HA showed a decline in its normalised modulus despite a similar compressive modulus at the foam phase. One reason for this decline could be an increase in Coll-HA density compared to Coll (16.4 kg/m^3 to 22.6 kg/m^3). Nevertheless, this result indicates that at a microscopic level, the local stiffnesses of the materials remained unchanged. While the exponent equalled to 2, the normalised compressive moduli of the solid phases of Coll-CS, Coll-HA and Coll-CS-HA were 0.89 ± 0.02 , 0.85 ± 0.10 and 0.73 ± 0.10 respectively. Coll-CS-HA in Fig. 3A had a lower normalised compressive modulus compared to in Fig. 3B. This was because the exponent of -2 overpowered the high compressive modulus, and thus appeared to be lower.

3.3 Alcian blue indicates the presence of HA in Coll-HA IPNs

Fig. 4 illustrates the histological staining by alcian blue of HA on Coll and two different concentration of HA IPNs: $0.75\%\text{Coll}-0.25\%\text{HA}$ and $0.5\%\text{Coll}-0.5\%\text{HA}$ by alcian blue. $0.75\%\text{Coll}-0.25\%\text{HA}$ was the Coll-HA used in other studies. Alcian blue is pH-controlled and stains that stained cations in GAGs in blue, and neural components, such as Coll, in grey.

Alcian blue staining indicated successful incorporation of HA onto Coll, as shown by the obvious blue branches on the surface of two Coll-HA scaffolds. Higher magnification images showed that HA networks could coexist with Coll struts and were also able to construct independent networks. This was shown by white arrowheads pointing to HA-rich regions and

black arrowheads pointing to Coll-rich regions. Blue struts on IPNs might not always indicate independent HA networks, as they may merely be HA forming over Coll branches.

Unsurprisingly, increasing HA concentrations on the IPNs led to an increased blue staining on the scaffolds. Comparing the two IPNs, 0.75%Coll-0.25%HA had more struts where both Coll and HA co-exist, which indicates that the HA concentration was low enough for exposing both Coll and HA. On 0.5%Coll-0.5%HA however, most struts, apart from the two black arrowheads, appeared to be completely blue.

3.4 IPNs decreased nestin expression

Cells seeded did not aggregate on the surface or at the edge of the scaffolds. Instead, colonies were distributed in uneven patterns throughout the scaffolds, indicating random infiltration and or migration of NSCs and their progeny. As shown in Fig. 5A, over a 21-day period, the percentage of nestin⁺ cells gradually declined in all scaffolds. This implies that the NSCs started differentiating and losing nestin expression, even though they were cultured in the presence of growth factors that stimulated NSC self-renewal. Coll-CS-HA showed significantly less nestin⁺ expression compared with Coll throughout the 21-day period. After D4, no nestin⁺ cells could be found on Coll-CS-HA at all, pointing to a higher degree of differentiation. Even at day 4, nestin expression on Coll-CS-HA was lower compared to other scaffolds. Coll, on the other hand, supported the largest number of nestin⁺ cell at day 4, where almost half of the cells expressed nestin. Coll-CS and Coll-HA however, only had around 20% nestin⁺ cells. At later time points, the percentage of nestin⁺ cells on Coll no longer become significantly higher than Coll-CS or Coll-HA. The final percentage of nestin⁺ cells at day 21 was $9\pm4\%$ for Coll, $7\pm3\%$ for Coll-CS and $6\pm5\%$ for Coll-HA respectively. There was no obvious difference in the percentage of cells expressing nestin on Coll-CS and Coll-HA. Both showed a gradual decline of nestin⁺ expression during the culture period. From day 7 to day 21 however, the decline was less significant.

PHi3 is a nuclear marker for proliferating cells. In order to qualitatively show the proliferative ability of SVZ stem and progenitor cells in the scaffolds, we co-stained nestin with PHi3 on Coll, Coll-CS and Coll-HA in proliferation media at 14 and 21 day in vitro (N=1). Co-expression of nestin and PHi3 is indicative of a proliferating stem cell. Coll-CS-HA is not shown because no nestin⁺ cells were found on that scaffold type at days 14 and 21. On the other scaffolds, many cells were found to express both nestin and PHi3 (Fig. 6). There were also cells expressing only PHi3 or nestin. These are likely proliferating neuroblasts or astrocytes, or nestin⁺ cells starting to differentiate. No primary controls showed only a weak background fluorescence from the secondary antibodies used (Fig. S2). A range of different intensities was observed with PHi3 staining, likely due to NSCs being at different stages of proliferation, as PHi3 only labels a small portion of the cell cycle (M phase).

3.5 Coll-CS induced higher GFAP expression

Glial fibrillary acidic protein (GFAP) is a classic marker of differentiated astrocytes. We found two astrocyte morphologies in our scaffolds, bipolar or stellate (Fig. S3). Bipolar astrocytes were GFAP⁺ cells with two processes emanating in opposite directions and stellate astrocytes were GFAP⁺ cells with three or more processes oriented in any direction vis-à-vis one another. We did not discern significant differences in astrocyte morphology in the different scaffolds (Fig. S5). Interestingly, the percentage of cells expressing GFAP on Coll-CS was significantly higher at

days 7, 14 and 21, compared to other scaffolds, by $38\pm 11\%$, $34\pm 1\%$ and $31\pm 6\%$, respectively (Fig. 7). Coll-CS also increased the percentage of GFAP⁺ cells to 37% at day 4, although this was not statistically significant compared to other scaffolds in which the percentage ranged from 25-27%. There were no obvious differences in the percentage of GFAP⁺ cells between Coll, Coll-HA and Coll-CS-HA at any of the time points (Fig. 7).

3.6 Map2 neuronal marker expression increases in scaffolds with IPN

Neuronal differentiation from NSCs was studied with two markers: Dcx, which is expressed by young neurons, and MAP2, which is expressed by mature neurons (Fig. 8). We used epidermal growth factor (EGF) and fibroblast growth factor (FGF) containing proliferation media here since TBIs are often associated with increased growth factor expression in the lesion and we sought to determine if scaffolds could support differentiation despite this. We found that approximately 10-20% of the cells on all scaffolds were Dcx⁺ (Fig. 8B). Interestingly, no significant differences in the percent of cells that expressed Dcx were seen across different scaffolds at any of the time points (Fig. 8B). Furthermore there was no significant change in the percent of Dcx⁺ cells throughout the 21-day period. The typical bipolar Dcx⁺ morphology remained similar in the scaffolds.

Fig. 8C illustrates quantification of MAP2⁺ cells on Coll and IPNs in proliferation media. On Coll-CS and Coll-HA, MAP2⁺ cells increased from $20\pm 5\%$ at day 14 to $25\pm 6\%$ and $27\pm 6\%$ at day 21, respectively, while the percentage of MAP2⁺ cells on Coll only slightly increased from $12\pm 2\%$ to $13\pm 1\%$. Enhancement in MAP2⁺ differentiation was similar in Coll-CS and Coll-HA. However, the addition of CS and HA did not induce a compound effect and in fact was less than with the other IPNs.

MAP2⁺ cells were also found on all scaffolds in differentiation media at 14- and 21-day post seeding (Fig. 9). Similar to their morphology in proliferation media, typical MAP2⁺ neurites were bipolar or stellate. Long extending neurites, both within the colonies and radiating out from them were more obvious in differentiation than in proliferation media. No nestin expression was observed in any of the scaffolds in differentiation media, signifying it was indeed inducing differentiation (not shown).

Supporting this, all three IPNs led to a significant increase in MAP2⁺ labelling at D14 in differentiation media (Fig 9B). The percentage MAP2⁺ was around 20% in Coll and increased to 30-40% in the IPNs at day 14 and day 21. On day 21, only Coll-HA showed a statistically significant increase compared to Coll. MAP2⁺ cells in differentiation compared to proliferation media, increased from $18\pm 2\%$ to $22\pm 6\%$ in Coll, and from ~20-25% to ~30-40% in IPNs. Cell death was eliminated as potentially contributing to these results as Caspase-3 staining showed limited cell death on all scaffolds (Fig. S4).

3. Discussion

In this study, we report a refined IPN synthesis method that successfully incorporates CS and/or HA into the Coll primary structure. The Coll-CS-HA tri-IPN structure was firstly synthesised and then tested on NSCs and reported here. The IPNs reduced nestin expression and

simultaneously increased MAP2+ expression, which could be beneficial for a tissue engineering-based brain therapy.

IPN strategies allow the manipulation of one network without affecting other networks in the same system. The crosslinking densities of HA and/or CS for example, could be easily altered without affecting Coll. The same applied to crosslinking of Coll, as dialysis can help remove crosslinking agents and avoid Coll crosslinking completely. If one wished to mix various materials in one step however, it would be more difficult to change the crosslinking density of one material without affecting the others.

Access of nutrients and oxygen throughout scaffolds and implants is a critical issue. Importantly, the porous nature of all our scaffolds made it likely that growth factors and other constituents of the cell culture media diffused evenly throughout the networks. Cell density was not so great as to block all the pores and thus, we cannot rule it out, but we do not believe that deeply located cells were exposed to different culture conditions than cells at scaffold surfaces. Nevertheless we controlled for such possible differences in nutrient diffusion across scaffolds by sampling cells at the same range of depths from the surface of the scaffolds.

Our IPN scaffolds attempted to avoid any chemical crosslinking between the primary and secondary networks, and linked the two networks by physical entanglement and attempted to achieve this in two steps. Firstly, excess amounts of EDC, NHS and ADH were used to crosslink HA and CS. This step aimed to react as many carboxylic acid groups as possible, thus forming an independent network before adding Coll. It is understandable that not all carboxylic acid groups would react due to physical impediment of the large molecules of HA and CS. Thus, we subsequently stored HA and CS solutions at 4°C overnight to ensure that EDC had lost most of its activity before Coll was added. Previous studies have demonstrated that, due to hydrolysis, the half-life of EDC in a pH 5 aqueous solution can be as low as 4 hrs [34].

The presence of HA and/or CS within the IPNs was confirmed by FTIR and histology. Alcian blue staining indicated the presence of HA and suggested the formation of HA secondary networks shown by the individual blue struts. Increasing HA concentration also led to an increase in the blue regions. This indicates the unique advantage of an IPN, that it was possible to alter the amount of HA without affecting Coll. In addition, FTIR spectra showed the presence of CS by the formation of new S-O-C peaks. It is worth noting that HA and CS are both water soluble materials. The presence of these GAGs after at least 3 hrs of stirring proved their capability of forming strong and stable networks.

The Gibson-Ashby equation is a commonly used approach to calculate the stiffness of porous materials. The constant local stiffnesses was expected as addition of an additional network should not alter the original primary network, or Coll. The measured stiffness should invariably depend on the individual stiffnesses of Coll or GAGs themselves. One previous study suggested that the mechanical properties of 1.0wt% Coll scaffold resembled rats' brains [36]. The local stiffness of interlaced networks was very similar to that of Coll and therefore their mechanical properties were within an appropriate range. The values for the compressive testing with exponent of 2 tended to be lower in the IPNs compared to collagen alone and was lowest on Coll-CS-HA, but these differences were not statistically significant. Compressive testing with exponent 3/2 also did not show statistically significant differences between the scaffolds. In this, and a few of our other experiments, it is possible that more replicates would have resulted in

statistical significance. Nevertheless, several of our studies, for example, the pore size of different scaffolds and the percentage of nestin⁺ cells in them, indeed showed significant differences. This indicated that the study in general was sufficiently powered.

The first phase of SVZ neurosphere culture is typically in the presence of EGF and FGF, which induce self-renewal, proliferation and survival of these cells. We included these media constituents (proliferation media) in the majority of experiments in order to induce robust growth of cultures in scaffolds. In the second phase of neurosphere culture, EGF and FGF are removed which induces differentiation. We used this “differentiation media” to assess the ability of different scaffolds to induce more complete neuronal differentiation (Map2⁺ vs TuJ1⁺). Remarkably, IPN scaffolds induced Map2 expression compared to Coll-alone. Additionally, the percentage of Map2⁺ cells was augmented in differentiation media compared to proliferation media, but only marginally so. These results suggest SVZ cells cultured in IPN scaffolds carry out robust differentiation despite culture conditions. Although the NSCs were provided with weekly addition of EGF and FGF in the “proliferation condition”, they lost significant nestin expression at Day 4 time in culture in the scaffolds containing IPNs. Surprisingly, no obvious nestin⁺ cells were found on the Coll-CS-HA scaffolds after day 4. It is reasonable to exclude cell death in this scenario, as Casp3 studies showed limited cell death on Coll-CS-HA scaffolds in the proliferation media. The lack of nestin⁺ expression may be due to the lack of exposed Coll on the scaffold, balancing most of the cells towards a differentiating phenotype. Another reason might be the small pore size of Coll-CS-HA, which allowed cells to fill the pore and lose nestin expression earlier as cells were in closer contact with the GAGs than on the other scaffold types. A combination of both scenarios could have contributed to the depletion of nestin⁺ cells.

Additionally, we showed that compared with the other scaffolds, the percentage of GFAP⁺ cells, showing astrocyte differentiation was significantly greater on Coll-CS. Moreover all three scaffolds with IPNs were able to increase the percent MAP2⁺ cells, indicating neuronal differentiation. Thus, addition of both and doubling the GAGs concentration could explain the depletion of nestin expression. This could have potential benefits as an implant, as transplantation of undifferentiated stem cells could lead to tumours or teratomas due to excessive growth of cells [37, 38]. There may have been other cell types in our scaffolds that we did not detect, since we did not discern the phenotype of 100% of cells. For example, at day 21 on Coll-CS in proliferation media, fewer than 10% of the cells were nestin⁺, about 30% were GFAP⁺ and about 25% were MAP2⁺. About 20% were Dcx⁺ (immature neurons) which may have partially overlapped with Map2 expression (mature neurons). We also detected some Olig2⁺ oligodendrocytes in these cultures (data not shown). Oligodendrocytes usually account for about 5% of cells in differentiated neurospheres [39]. Some cells may have been undifferentiated in the experiments carried out in proliferation media which typically maintains stem cells and progenitors but constrains differentiation. A variety of progenitors have been found in single cell RNAseq studies of the SVZ [40, 41] and it is possible that some progenitor cells did not express immunodetectable nestin or GFAP, accounting for at least some of the marker-negative cells in these studies.

CSPG is a component of scars formed after CNS injury [24] and of CNS cancers [42]. A major constituent of glial scars are reactive astrocytes that express high levels of GFAP. This is commensurate with our finding of high GFAP expression levels in Coll-CS scaffolds. Although Coll-CS led to the highest percentage of GFAP⁺ cells (30-40%) throughout the 21 days, the percentage

on Coll-CS-HA remained unchanged. This was likely because high-molecular weight HA inhibited astrocytic differentiation, as a similar effect has been observed in vivo [43]. There was no significant increase in GFAP+ labelling from day 4 to day 21 on all scaffolds. This may be due to astrocyte differentiation taking place rapidly within the first 4 days and then was maintained. Comparing the decline in nestin from day 4 to day 7, it can be extrapolated that many of the nestin+ cells might have directly differentiated into or given rise to astrocytes. Possibly due to previous findings of CS inhibiting neurite outgrowth [44], there are few studies [45] using CS as a potential therapy for TBI compared to Coll and HA. Our study provided another possible drawback for using CS, which is its ability to enhance astrocytic differentiation. Astrocytes have secrete CSPG and HSPG in vivo, which later form glial scars that prevent neural regeneration after a TBI [25, 46].

Similar to previous studies, many of the MAP2+ cells found on scaffolds were either monopolar or bipolar, indicating a relatively immature phenotype even in the differentiation media [11]. Cells with clearly distinguishable morphology tended to be either isolated or surrounded by MAP2-negative cells. However, morphological studies proved to be difficult due to the 3D shape of the scaffolds and the high cell density. The mechanism of enhanced MAP2+ expression on Coll-HA scaffolds could be due to clustered of differentiation 44 (CD44), which is a surface receptor that binds to HA via its amino-terminal domain [47]. Previous studies discovered that the removal of CD44 in mouse brains enhanced proliferation and delayed neuronal differentiation from Dcx+ to NeuN+, another mature neuronal marker [48]. This is consistent with our finding that the Dcx+ population did not change but that mature marker MAP2+, was elevated. Previous studies have discovered that CD44 is essential for Wnt-induced activation and nuclear translocation of β -catenin, since down- or upregulation of CD44 was directly related to a decrease or increase of Wnt/ β -catenin signalling [49, 50]. Thus, the effect of HA-CD44 on neuronal differentiation may rely on the Wnt signalling pathway, an important signaling cascade throughout brain development and formation of neuronal circuits. The fact that both Coll-CS and Coll-HA enhanced MAP2+ expression to approximately the same level, while keeping Dcx+ expression almost unaffected, implies that the mechanism behind neuronal differentiation may have been similar, if not the same. Although not much has been investigated concerning functional links between CS and Wnt signalling in the CNS, previous research has showed that digesting C6S in articular cartilage by ChABC reduced the chondrocyte response to Wnt signalling [51]. Hence, it is possible that CS might have improved neuronal differentiation via a similar biological mechanism. Furthermore, although CD44 is a common surface receptor for HA, it also readily binds to CS [52-54]. Thus, CS might enhance MAP2+ expression via a similar CD44-Wnt signalling pathway.

The studies presented here were informative in determining how NSCs respond in vitro to 3D scaffolds with different compositions. Considering they induced GFAP less than Coll-CS, Coll-HA and Coll-CS-HA seem to be the two optimal scaffolds for subsequent animal studies. Although all three IPNs had similar effects on neuronal differentiation, Coll-HA and Coll-CS-HA did not induce higher GFAP+ differentiation. However, future studies of Coll-CS-HA might need to consider its compressive modulus, as the force it exerts onto the surrounding tissue after implantation may cause distortion of the injured tissue and worsen intracranial hypertension, a common side effect of TBI [55]. It is known that different parts of the brain have different stiffness. For example, white matter is thought to be stiffer than grey matter [56, 57]. Implantation into different regions, therefore, may require personalised scaffolds to match the

composition and mechanical properties of the implanted brain area. In the future, we also envision moulding scaffolds to match the size and shape of individual TBIs.

Other groups have generated HA-containing IPNs and semi-interpenetrating networks which gave control over their mechanical properties and were compatible with peripheral nervous system (PNS) Schwann cells [58]. Additionally laminin and fibronectin have been incorporated into collagen 1 and HA IPN's and controlled PNS neurite extension [59]. Collagen-HA IPNs reduce glioblastoma infiltration [60]. A mixed IPN of Coll-CS-HA had tuneable biophysical properties and was compatible with chondrocytes and regulated their secretion of GAGs and collagen II [61]. Thus an emerging literature suggests that a variety of IPN combinations can regulate multiple biological responses in different cells.

4. Conclusions

In this study, we fabricated three collagen-based IPN scaffolds: Coll-CS, Coll-HA and Coll-CS-HA, and compared the physical and biological properties with Coll alone scaffolds. The synthesis was successful in incorporating the secondary networks of GAGs onto Coll. The IPNs were all capable of inducing high MAP2+ expression in both proliferation and differentiation media. However, Coll-CS alone led to higher GFAP+ expression, which may lead to detrimental effects such as glial scar formation. Nestin expression was higher on Coll alone than on scaffolds with IPNs, implying it maintained a stem cell phenotype. All IPNs induced a significant decline in nestin+ expression. In fact, no nestin+ cells were found on Coll-CS-HA after 4 days in proliferation media, which may be advantageous as implanting stem cells could induce tumours or teratomas. Overall, we believe that Coll-HA and Coll-CS-HA may be the most suitable candidates for brain tissue engineering therapy.

Acknowledgements

This research did not receive any specific grant from funding agencies in the public, commercial, or not-for-profit sectors.

References

- [1] t.b.i.a. Headway, Brain injury statistics, 2015. <https://www.headway.org.uk/brain-injury-statistics.aspx>. (Accessed 25/09 2015).
- [2] B.T. Foundation, TBI Statistics, Facts About TBI in the USA, 2015. <https://www.braintrauma.org/tbi-facts/tbi-statistics/>.
- [3] K. Jaracz, B. Grabowska-Fudala, K. Górna, W. Kozubski, Consequences of stroke in the light of objective and subjective indices: A review of recent literature, *Neurol. Neurochir. Pol.* 48 (2014) 280-286.

- [4] H. Ling, J. Hardy, H. Zetterberg, Neurological consequences of traumatic brain injuries in sports, *Molecular and Cellular Neuroscience* 66 (2015) 114-122.
- [5] C. Lois, A. Alvarez-Buylla, Long-distance neuronal migration in the adult mammalian brain, *Science* 264(5162) (1994) 1145-1148.
- [6] D.G. Herrera, J.M. Garcia - Verdugo, A. Alvarez - Buylla, Adult - derived neural precursors transplanted into multiple regions in the adult brain, *Annals of Neurology* 46(6) (1999) 867-877.
- [7] R. Seidenfaden, A. Desoeuvre, A. Bosio, I. Virard, H. Cremer, Glial conversion of SVZ-derived committed neuronal precursors after ectopic grafting into the adult brain, *Molecular and Cellular Neuroscience* 32(1) (2006) 187-198.
- [8] K.K. Meissner, D.L. Kirkham, L.C. Doering, Transplants of neurosphere cell suspensions from aged mice are functional in the mouse model of Parkinson's, *Brain Research* 1057(1) (2005) 105-112.
- [9] M.A. Lancaster, J.A. Knoblich, Generation of cerebral organoids from human pluripotent stem cells, *Nature Protocols* 9 (2014) 2329.
- [10] J. Ogawa, G.M. Pao, M.N. Shokhirev, I.M. Verma, Glioblastoma Model Using Human Cerebral Organoids, *Cell Reports* 23(4) (2018) 1220-1229.
- [11] S. Koutsopoulos, S. Zhang, Long-term three-dimensional neural tissue cultures in functionalized self-assembling peptide hydrogels, Matrigel and Collagen I, *Acta biomaterialia* 9 (2013) 5162-5169.
- [12] J. Zhong, A. Chan, L. Morad, H.I. Kornblum, G. Fan, S.T. Carmichael, Hydrogel Matrix to Support Stem Cell Survival After Brain Transplantation in Stroke, *Neurorehabilitation and neural repair* 24(7) (2010) 636-644.
- [13] F.G. Szele, M.F. Chesselet, Cortical lesions induce an increase in cell number and PSA-NCAM expression in the subventricular zone of adult rats, *J Comp Neurol* 368(3) (1996) 439-54.
- [14] E.H. Chang, I. Adorjan, M.V. Mundim, B. Sun, M.L. Dizon, F.G. Szele, Traumatic Brain Injury Activation of the Adult Subventricular Zone Neurogenic Niche, *Front Neurosci* 10 (2016) 332.
- [15] B. Saha, S. Peron, K. Murray, M. Jaber, A. Gaillard, Cortical lesion stimulates adult subventricular zone neural progenitor cell proliferation and migration to the site of injury, *Stem Cell Res* 11(3) (2013) 965-977.
- [16] L.W. Lau, R. Cua, M.B. Keough, S. Haylock-Jacobs, V.W. Yong, Pathophysiology of the brain extracellular matrix: a new target for remyelination, *Nature Review* 14 (2013) 722-729.
- [17] C. Lindwall, M. Olsson, A.M. Osman, H.G. Kuhn, M.A. Curtis, Selective expression of hyaluronan and receptor for hyaluronan mediated motility (Rhamm) in the adult mouse subventricular zone and rostral migratory stream and in ischemic cortex, *Brain Research* 1503 (2013) 62-77.
- [18] L.B. Thomas, M.A. Gates, D.A. Steindler, Young neurons from the adult subependymal zone proliferate and migrate along an astrocyte, extracellular matrix-rich pathway, *Glia* 17(1) (1996) 1-14.

- [19] N. Sanai, T. Nguyen, R.A. Ihrie, Z. Mirzadeh, H.H. Tsai, M. Wong, N. Gupta, M.S. Berger, E. Huang, J.M. Garcia-Verdugo, D.H. Rowitch, A. Alvarez-Buylla, Corridors of migrating neurons in the human brain and their decline during infancy, *Nature* 478(7369) (2011) 382-6.
- [20] M.A. Curtis, M. Kam, U. Nannmark, M.F. Anderson, M.Z. Axell, C. Wikkelso, S. HoltÅs, W.M. van Roon-Mom, T. Björk-Eriksson, C. Nordborg, J. FrisÈn, M. Dragunow, R.L. Faull, P.S. Eriksson, Human neuroblasts migrate to the olfactory bulb via a lateral ventricular extension, *Science* 315(5816) (2007) 1243-9.
- [21] K. Sawamoto, Y. Hirota, C. Alfaro-Cervello, M. Soriano-Navarro, X. He, Y. Hayakawa-Yano, M. Yamada, K. Hikishima, H. Tabata, A. Iwanami, K. Nakajima, Y. Toyama, T. Itoh, A. Alvarez-Buylla, J.M. Garcia-Verdugo, H. Okano, Cellular composition and organization of the subventricular zone and rostral migratory stream in the adult and neonatal common marmoset brain, *J Comp Neurol* 519(4) (2011) 690-713.
- [22] J. Lam, W.E. Lowry, S.T. Carmichael, T. Segura, Hyaluronic acid matrix promotes the differentiation of transplanted cells, *Advanced functional materials* 24 (2014) 7053-7062.
- [23] S. Hou, Q. Xu, W. Tian, F. Cui, Q. Cai, J. Ma, I.-S. Lee, The repair of brain lesion by implantation of hyaluronic acid hydrogels modified with laminin, *Journal of Neuroscience Methods* 148(1) (2005) 60-70.
- [24] F. Barnabé-Heider, C. Göritz, H. Sabelström, H. Takebayashi, F.W. Pfrieger, K. Meletis, J. Frisén, Origin of New Glial Cells in Intact and Injured Adult Spinal Cord, *Cell Stem Cell* 7(4) (2010) 470-482.
- [25] C.M. Galtrey, J.W. Fawcett, The role of chondroitin sulfate proteoglycans in regeneration and plasticity in the central nervous system, *Brain Research Reviews* 54 (2007) 1-18.
- [26] P.Z. Elias, M. Spector, Implantation of a collagen scaffold seeded with adult rat hippocampal progenitors in a rat model of penetrating brain injury, *J. Neurosci. Methods* 209 (2012) 199-211.
- [27] K.-F. Huang, W.-C. Hsu, W.-T. Chiu, J.-y. Wang, Functional improvement and neurogenesis after collagen-GAG matrix implantation into surgical brain trauma, *Biomaterials* 33 (2012) 2067-2075.
- [28] Y. Ni, Z. Tang, W. Cao, H. Lin, Y. Fan, L. Guo, X. Zhang, Tough and elastic hydrogel of hyaluronic acid and chondroitin sulfate as potential cell scaffold materials, *Int. J. Biol. Macromol.* 74 (2015) 367-375.
- [29] I.V. Yannas, Emerging rules for inducing organ regeneration, *Biomaterials* 34(2) (2013) 321-30.
- [30] B.d.C. Vidal, M.L.S. Mello, FT-IR Microspectroscopy of Rat Ear Cartilage, *PLoS ONE* 11(3) (2016).
- [31] A. Lungu, M.G. Albu, N.M. Florea, I.C. Strancu, E. Vasile, H. Iovu, The influence of glycosaminoglycan type on the collagen-glycosaminoglycan porous scaffolds, *Digest Journal of Nanomaterials and Biostructures* 6(4) (2011) 1867-1875.
- [32] K.T. Mader, M. Peeters, S.E.L. Detiger, M.N. Helder, T.H. Smit, Christine L. Le Maitre, C. Sammona, Investigation of intervertebral disc degeneration using multivariate FTIR spectroscopic imaging, *Faraday Discussions* 187(1) (2016) 393-414.

- [33] M. Tamaddon, R.S. Walton, D.D. Brand, J.T. Czernuszka, Characterisation of freeze-dried type II collagen and chondroitin sulfate scaffolds, *J Mater Sci: Mater Med* 24 (2013) 1153–1165.
- [34] S.M.D.G. Plepis, G. Goisis, D.K. Das-Gupta, Dielectric and Pyroelectric Characterization of Anionic and Native Collagen, *Polymer Engineering and Science* 36(24) (1996) 2932–2938.
- [35] K. Pietrucha, Physicochemical properties of 3D collagen-CS scaffolds for potential use in neural tissue engineering, *Int. J. Biol. Macromol.* 80 (2015) 732–739.
- [36] P.Z. Elias, M. Spector, Viscoelastic characterization of rat cerebral cortex and type I collagen scaffolds for central nervous system tissue engineering, *J Mech Behav Biomed Mater* 12 (2012) 63–73.
- [37] C.E. Murry, G. Keller, Differentiation of Embryonic Stem Cells to Clinically Relevant Populations: Lessons from Embryonic Development, *Cell* 132(4) (2008) 661–680.
- [38] J. Nussbaum, Elina Minami, M.A. Laflamme, Jitka A. I. Virag, C.B. Ware, A. Masino, V. Muskheli, L. Pabon, H. Reinecke, C.E. Murry, Transplantation of undifferentiated murine embryonic stem cells in the heart: teratoma formation and immune response, *The FASEB Journal* 21(7) (2007) 1345–1357.
- [39] B. Sun, E. Chang, A. Gerhartl, F.G. Szele, Polycomb Protein Eed is Required for Neurogenesis and Cortical Injury Activation in the Subventricular Zone, *Cereb Cortex* 28(4) (2018) 1369–1382.
- [40] B.W. Dulken, D.S. Leeman, S.C. Boutet, K. Hebestreit, A. Brunet, Single-Cell Transcriptomic Analysis Defines Heterogeneity and Transcriptional Dynamics in the Adult Neural Stem Cell Lineage, *Cell reports* 18(3) (2017) 777–790.
- [41] D. Mizrak, H.M. Levitin, A.C. Delgado, V. Crotet, J. Yuan, Z. Chaker, V. Silva-Vargas, P.A. Sims, F. Doetsch, Single-Cell Analysis of Regional Differences in Adult V-SVZ Neural Stem Cell Lineages, *Cell reports* 26(2) (2019) 394–406 e5.
- [42] D.J. Silver, F.A. Siebzehnrbuhl, M.J. Schildts, A.T. Yachnis, G.M. Smith, A.A. Smith, B. Scheffler, B.A. Reynolds, J. Silver, D.A. Steindler, Chondroitin Sulfate Proteoglycans Potently Inhibit Invasion and Serve as a Central Organizer of the Brain Tumor Microenvironment, *J Neurosci* 33(39) (2013) 15603–15617.
- [43] Z.K. Zin, D.M. Brian, E.V. Jennifer, K.S. Stephanie, J.G. Raymond, E.S. Christine, High molecular weight hyaluronic acid limits astrocyte activation and scar formation after spinal cord injury, *Journal of Neural Engineering* 8(4) (2011) 046033.
- [44] C.M. Galtrey, J.W. Fawcett, The role of chondroitin sulfate proteoglycans in regeneration and plasticity in the central nervous system, *Brain Res Rev* 54(1) (2007) 1–18.
- [45] M.I. Betancur, H.D. Mason, M. Alvarado-Velez, P.V. Holmes, R.V. Bellamkonda, L. Karumbaiah, Chondroitin Sulfate Glycosaminoglycan Matrices Promote Neural Stem Cell Maintenance and Neuroprotection Post-Traumatic Brain Injury, *ACS Biomater Sci Eng* 3(3) (2017) 420–430.
- [46] S.M. Dyck, S. Karimi-Abdolrezaee, Chondroitin sulfate proteoglycans: Key modulators in the developing and pathologic central nervous system, *Experimental Neurology* 269 (2015) 169–187.

- [47] H. Ponta, L. Sherman, P.A. Herrlich, CD44: From adhesion molecules to signalling regulators, *Nature Reviews Molecular Cell Biology* 4 (2003) 33.
- [48] W. Su, S.C. Foster, R. Xing, K. Feistel, R.H.J. Olsen, S.F. Acevedo, J. Raber, L.S. Sherman, CD44 Transmembrane Receptor and Hyaluronan Regulate Adult Hippocampal Neural Stem Cell Quiescence and Differentiation, *Journal of Biological Chemistry* 292(11) (2017) 4434-4445.
- [49] M. Schmitt, The role of CD44 in Wnt/ β -catenin signaling, Fakultät für Chemie und Biowissenschaften, Karlsruher Institut für Technologie 2014, p. 164.
- [50] M. Schmitt, M. Metzger, D. Gradl, G. Davidson, V. Orian-Rousseau, CD44 functions in Wnt signaling by regulating LRP6 localization and activation, *Cell Death And Differentiation* 22 (2014) 677.
- [51] S. Shortkroff, K.E. Yates, Alteration of matrix glycosaminoglycans diminishes articular chondrocytes' response to a canonical Wnt signal, *Osteoarthritis and Cartilage* 15(2) (2007) 147-154.
- [52] T. Fujimoto, H. Kawashima, T. Tanaka, M. Hirose, N. Toyama-Sorimachi, Y. Matsuzawa, M. Miyasaka, CD44 binds a chondroitin sulfate proteoglycan, aggrecan, *International Immunology* 13(3) (2001) 359-66.
- [53] E. Hurt-Camejo, B. Rosengren, P. Sartipy, K. Elfsberg, G. Camejo, L. Svensson, CD44, a Cell Surface Chondroitin Sulfate Proteoglycan, Mediates Binding of Interferon- γ and Some of Its Biological Effects on Human Vascular Smooth Muscle Cells, *Journal of Biological Chemistry* 274(27) (1999) 18957-18964.
- [54] C.A. Henke, U. Roongta, D.J. Mickelson, J.R. Knutson, J.B. McCarthy, CD44-related chondroitin sulfate proteoglycan, a cell surface receptor implicated with tumor cell invasion, mediates endothelial cell migration on fibrinogen and invasion into a fibrin matrix, *The Journal of Clinical Investigation* 97(11) (1996) 2541-2552.
- [55] P.L. Roux, Intracranial Pressure Monitoring and Management, in: D. Laskowitz, G. Grant (Eds.), *Translational Research in Traumatic Brain Injury*, CRC Press/Taylor and Francis Group, Boca Raton, 2016.
- [56] T. Kaster, I. Sack, A. Samani, Measurement of the hyperelastic properties of ex vivo brain tissue slices, *Journal of Biomechanics* 44(6) (2011) 1158-1163.
- [57] J.A.W. van Dommelen, T.P.J. van der Sande, M. Hrapko, G.W.M. Peters, Mechanical properties of brain tissue by indentation: Interregional variation, *Journal of the Mechanical Behavior of Biomedical Materials* 3(2) (2010) 158-166.
- [58] S. Suri, C.E. Schmidt, Photopatterned collagen-hyaluronic acid interpenetrating polymer network hydrogels, *Acta biomaterialia* 5(7) (2009) 2385-97.
- [59] C. Deister, S. Aljabari, C.E. Schmidt, Effects of collagen 1, fibronectin, laminin and hyaluronic acid concentration in multi-component gels on neurite extension, *J Biomater Sci Polym Ed* 18(8) (2007) 983-97.
- [60] S.S. Rao, J. Dejesus, A.R. Short, J.J. Otero, A. Sarkar, J.O. Winter, Glioblastoma behaviors in three-dimensional collagen-hyaluronan composite hydrogels, *ACS Appl Mater Interfaces* 5(19) (2013) 9276-84.

[61] Y. Guo, T. Yuan, Z. Xiao, P. Tang, Y. Xiao, Y. Fan, X. Zhang, Hydrogels of collagen/chondroitin sulfate/hyaluronan interpenetrating polymer network for cartilage tissue engineering, *J Mater Sci Mater Med* 23(9) (2012) 2267-79.

Figure Legends

Figure 1. SEM images and pore size analysis of scaffolds. A) SEM images of scaffold cross-sections and higher magnification images showing open pores and secondary pores structure (white arrowheads). B) Higher magnification SEM images of Coll-CS-HA showing an overall more distorted pore structure and a higher magnification image that reveals extensive struts in between pores and forming secondary pores, as indicated by white arrowheads. C) Average pore size of Coll and IPN scaffolds measured by ImageJ. Results are presented as mean \pm standard deviation. Overlapping bar charts showing comparisons of pore size distributions between Coll and D) Coll-CS, E) Coll-HA, and F) Coll-CS-HA. (n=3) (**p<0.005, ***p<0.0005).

Figure 2. A) FTIR spectra of IPNs and Coll superimposed from 1000 cm^{-1} to 4000 cm^{-1} . B) FTIR spectra of IPNs and Coll from 1000 cm^{-1} to 1100 cm^{-1} . C) FTIR spectra from 1500 cm^{-1} to 1700 cm^{-1} showing amide I and amide II. D) FTIR spectra from 2750 cm^{-1} to 3050 cm^{-1} showing amide B. E) FTIR spectra of IPNs and Coll from 3200 cm^{-1} to 3400 cm^{-1} . F) Second derivatives of FTIR spectra.

Figure 3. Compressive testing. Elastic moduli of the solid phases of scaffolds normalised to Coll, calculated by the Gibson-Ashby equation, where the exponent equals to A) 3/2, and B) 2 respectively. Error bars indicate \pm standard deviation. (n=3). (n.s. = non-significant).

Figure 4. Histology studies using alcian blue for analysis of HA on Coll, 0.75%Coll-0.25%HA and 0.5%Coll-0.5%HA. A) Slices of scaffolds under a light microscope at a lower magnification. B) Higher magnification images of A) showing more detailed microstructure. C) Higher magnification images of B) showing individual struts of scaffolds. Alcian blue stains HA in blue, and Coll in grey. Black arrowheads point to Coll and white arrowheads point to HA.

Figure 5. A) Representative confocal images of immunocytochemistry showing nestin+ cells on Coll and IPNs at day 4, 7, 14 and 21 after seeding in proliferation media. Images were taken at 63x. Blue: DAPI and red: nestin. B) Quantification of nestin+ cells as a percentage of DAPI. Arrowheads pointing at non-detectable nestin in the Coll-CS-HA networks at day 7-21. Error bars indicate \pm standard deviation. (n=3) (*p<0.05).

Figure 6. Nestin and PHi3 co-labelling on Coll, Coll-CS and Coll-CS-HA scaffolds at day 14 and 21 after seeding in proliferation media. White: PHi3+ and red: nestin+. White arrowheads point to co-labelled cells. Quantification was not done as only one Phi3 staining was carried out.

Figure 7. A) Representative confocal images of GFAP+ cells on Coll and IPNs at days 4, 7, 14 and 21 after seeding in proliferation media. Images were taken at 63x. Blue: DAPI and green: GFAP. B) Quantification of GFAP+ cells as a percentage of DAPI. Error bars indicate \pm standard deviation. (n=3) (*p<0.05, **p<0.005, ***p<0.0005).

Figure 8. A) Representative confocal images of Dcx+ cells on Coll and IPNs at days 4 and 7, and Dcx+ and MAP2+ cells at days 14 and 21 after seeding in proliferation media. Images were taken at 63x. Blue: DAPI, green: MAP2 and red: Dcx. B) Quantification of Dcx+ cells as a percentage of DAPI. C) Quantification of MAP2+ cells as a percentage of DAPI. Error bars indicate \pm standard deviation. (n=3) (*p<0.05).

Figure 9. A) Representative confocal images of MAP2+ cells at day 14 and 21 after seeding in differentiation media. Images were taken at 63x. Blue: DAPI and green: MAP2. B) Quantification of MAP2+ cells as a percentage of DAPI. Error bars indicate \pm standard deviation. (n=3) (*p<0.05, **p<0.005)

Graphical Abstract

Engineered scaffolds can regulate neural stem cell proliferation and fate. To test this in subventricular zone stem cells, we made scaffolds of collagen alone (Coll), collagen-chondroitin sulfate (Coll-CS), collagen-hyaluronic acid (Coll-HA) and collagen-chondroitin sulfate-hyaluronic acid (Coll-CS-HA). Compared to Coll alone, the other scaffolds decreased the percent of Nestin+ stem cells and increased the percent of Map2+ neurons. Coll-CS also increased the percent of GFAP+ astrocytes. (Note the scaffolds are rendered opaque and cell types pseudocolored for clarity.)

<!--insert-fig-->